frontiers in Chemistry

ORIGINAL RESEARCH
published: 03 September 2020
doi: 10.3389/fchem.2020.00773

Fabrication of Er^{3+}/Yb^{3+} Co-Doped Bi_5O_7I Microsphere With Upconversion Luminescence and Enhanced Photocatalytic Activity for Bisphenol A Degradation

*Baowei Cao[1], Siwen Gong[2], Siyaka Mj Zubairu[3], Lingna Liu[1], Yunhua Xu[1], Lei Guo[1], Rui Dang[1] and Gangqiang Zhu[1,2]**

[1] School of Chemistry and Chemical Engineering, Yulin University, Yulin, China, [2] School of Physics and Information Technology, Shaanxi Normal University, Xi'an, China, [3] Department of Chemistry, Federal University Gashua, Gashua, Nigeria

Er^{3+}/Yb^{3+} co-doped Bi_5O_7I uniform porous microsphere photocatalysts were synthesized by a two-step chemical method, which possesses excellent photocatalytic performance and upconversion luminescence property. The photocatalytic performance of the photocatalysts was studied by degradation of bisphenol A in aqueous solution under visible light and different monochromatic light irradiation. The photocatalytic performance of Er^{3+}/Yb^{3+} co-doped Bi_5O_7I sample is better than that of the pristine Bi_5O_7I and Er^{3+}-doped Bi_5O_7I samples. Moreover, Er^{3+}/Yb^{3+} co-doped Bi_5O_7I possesses photocatalytic ability with a red light monochromatic LED lamp (3 W, $\lambda = 630$ nm) and an infrared monochromatic LED lamp (100 W, $\lambda = 940$ nm) irradiation whose wavelength is longer than the absorption-limiting wavelength of pristine Bi_5O_7I sample. This phenomenon further verified that the upconversion property of Er^{3+} and Yb^{3+} causes the improved photocatalytic efficiency of Er^{3+}/Yb^{3+} co-doped Bi_5O_7I sample.

Keywords: doping, semiconductor, microsphere, upconversion, heterojunction photocatalytic activity, NO removal, Rhodamine B

OPEN ACCESS

Edited by:
Shijie Li,
Zhejiang Ocean University, China

Reviewed by:
Zhifeng Liu,
Tianjin Chengjian University, China
Junbo Zhong,
Sichuan University of Science and Engineering, China

***Correspondence:**
Gangqiang Zhu
zgq2006@snnu.edu.cn

Specialty section:
This article was submitted to Catalysis and Photocatalysis, a section of the journal Frontiers in Chemistry

Received: *26 June 2020*
Accepted: *24 July 2020*
Published: *03 September 2020*

Citation:
Cao B, Gong S, Zubairu SM, Liu L, Xu Y, Guo L, Dang R and Zhu G (2020) Fabrication of Er^{3+}/Yb^{3+} Co-Doped Bi_5O_7I Microsphere With Upconversion Luminescence and Enhanced Photocatalytic Activity for Bisphenol A Degradation. Front. Chem. 8:773. doi: 10.3389/fchem.2020.00773

INTRODUCTION

Upconversion is a particular type of photoluminescence (PL), which converts low-energy excitation light into high-energy emission light through a multiphoton absorption process (Obregón and Colón, 2014a; Chuai et al., 2015; Ma et al., 2015; Fu et al., 2017). For this excellent characteristic, many upconverting materials, such as YF_3 and $NaYF_4$, have been used as powerful assistants to combine with semiconductor photocatalysts to improve light utilization recently (Huang et al., 2012; Li et al., 2013). For instance, Qin et al. (2010) reported that the graphene-supported $NaYF_4$:Yb^{3+}, Tm^{3+}, and N-doped P25 nanocomposite photocatalysts exhibit outstanding photocatalytic efficiency, because upconverting materials can effectively convert long-wavelength infrared (IR) light into short-wavelength light (such as visible light). The semiconductors in the composite photocatalysts can absorb the converted short-wavelength light to make full use of incident light. However, many up-conversion materials did not have photocatalytic performance because of their large band gap (Wang et al., 2013; Xu et al., 2013). Therefore, it is important to fabricate single-phase photocatalyst with excellent photocatalytic activity and upconversion property.

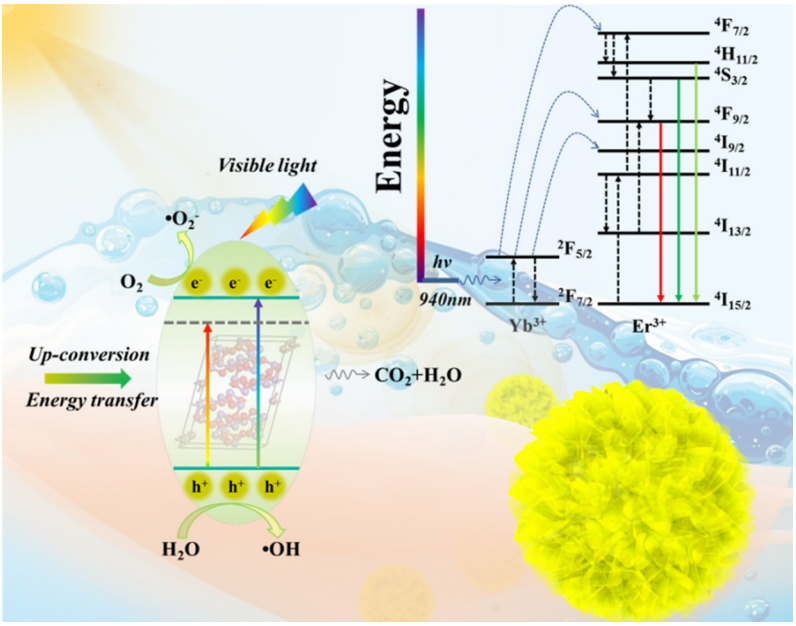

GRAPHICAL ABSTRACT | Er^{3+}/Yb^{3+} co-doped Bi_5O_7I porous microsphere photocatalysts show efficiency photocatalytic properties for bisphenol A degradation under visible and near-infrared light irradiation.

Bi_5O_7I as a novel semiconductor photocatalytic material with an optical band gap of ∼2.8 eV has received a lot of attention (Zhang et al., 2020a). The lamellar crystallographic structure of Bi_5O_7I can form an internal electrostatic field whose direction is vertical to the atom layer. The internal electrostatic field can promote the separation of photo-generated electron-hole pairs (Lan et al., 2020). However, the shortcomings of low light absorption and transmission efficiency of carriers still limit its photocatalytic activity. It is well-known that combining Bi_5O_7I with other semiconductors to form heterojunction could improve the separation rate of photo-generated charge carriers and show enhanced photocatalytic efficiency for pollutants degradation (Liu et al., 2015; Zhang et al., 2020b). In addition, our previous report indicated that the doping of Er^{3+} into the Bi_5O_7I can broaden the photo-response range due to the upconversion effect (Hojamberdiev et al., 2020), but the light conversion is not thorough enough. It can be inferred that the Er^{3+}/Yb^{3+} co-doping would cause more intensive upconversion fluorescence effect (Ding et al., 2016), which can enhance photocatalytic degradation properties for pollutions with full spectral solar light response.

In this work, uniform Er^{3+}/Yb^{3+} co-doped Bi_5O_7I microsphere photocatalysts were prepared by a two-step hydrothermal and thermal–decomposition method. The as-prepared photocatalysts have excellent photocatalytic performance and upconversion luminescence property. From the results of photocatalytic performance tests under the illumination of visible and monochromatic light and trapping experiments, the detailed mechanism of improved photocatalytic activity was also proposed.

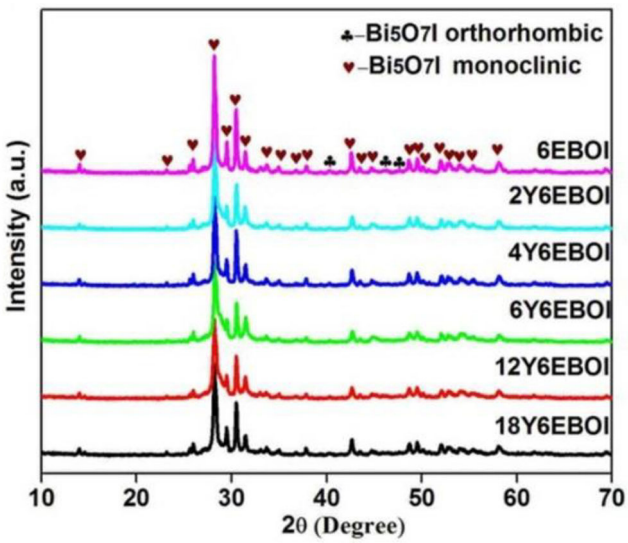

FIGURE 1 | XRD patterns of 6EBOI, 2Y6EBOI, 4Y6EBOI, 6Y6EBOI, 12Y6EBOI, and 18Y6EBOI samples.

EXPERIMENTAL

The synthesis methods of Bi_5O_7I and 6%Er^{3+}-doped Bi_5O_7I samples are detailed in the **Supporting Information** and the prepared samples were recorded as BOI and 6EBOI, respectively. In addition, the synthesis method

of Yb^{3+}/Er^{3+} co-doped Bi_5O_7I samples was similar to that previously reported (Zhang et al., 2019), except the addition of 2 to 18% $Yb(NO_3)_3$ $6H_2O$. The prepared samples were recorded as 2Y6EBOI, 4Y6EBOI, 6Y6EBOI, 12Y6EBOI, and 18YEBOI, respectively. The characterization and photocatalytic test are also described in the **Supporting Information**.

RESULTS AND DISCUSSION

XRD Analysis

The XRD patterns of 6EBOI and YEBOI samples are shown in **Figure 1**, and all the prepared samples are crystallized well. As previously reported, the Bi_5O_7I synthesized without any doping corresponds with orthorhombic phase Bi_5O_7I (JCPDS

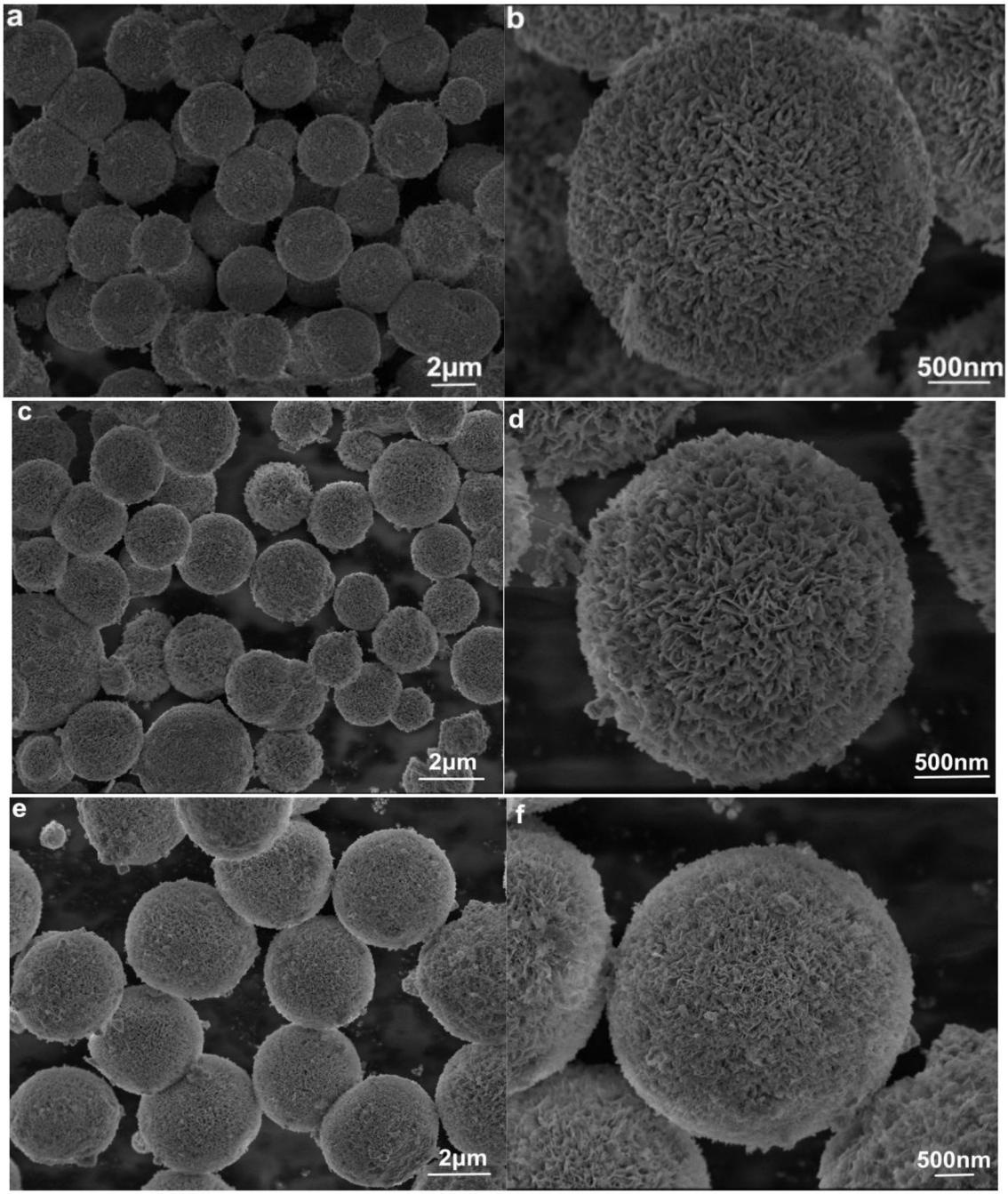

FIGURE 2 | SEM images of BOI **(a,b)**, 6EBOI **(c,d)**, and 6Y6EBOI **(e,f)** samples.

40-0548) (Hojamberdiev et al., 2020). However, the synthesized 6EBOI sample is in accordance with orthorhombic phase Bi_5O_7I and monoclinic phase (JCPDS 38-0669) Bi_5O_7I. In addition, the phase structure of the samples is completely converted into monoclinic Bi_5O_7I after doping with Yb^{3+}. Moreover, as the Yb^{3+} doping content increases, the width of these peaks broadens and the intensity decreases, especially the (004) peak. This is because the doping of Yb^{3+} and Er^{3+} limits the growth of Bi_5O_7I crystals. According to the previous reports, the existence of Yb^{3+} and Er^{3+} in the compound can cause phase transition from the orthorhombic phase to the monoclinic phase (Lin et al., 2014; Obregón and Colón, 2014b; Obregón et al., 2014).

Scanning Electron Microscope Analysis

Figure 2 displays the scanning electron microscope (SEM) images of the synthesized pure BOI, 6EBOI, and YEBOI samples. As shown in **Figure 2a**, the BOI sample has a uniform porous spherical morphology with a radius in the range of 1 to 1.5 μm. From **Figure 2b**, the high-resolution

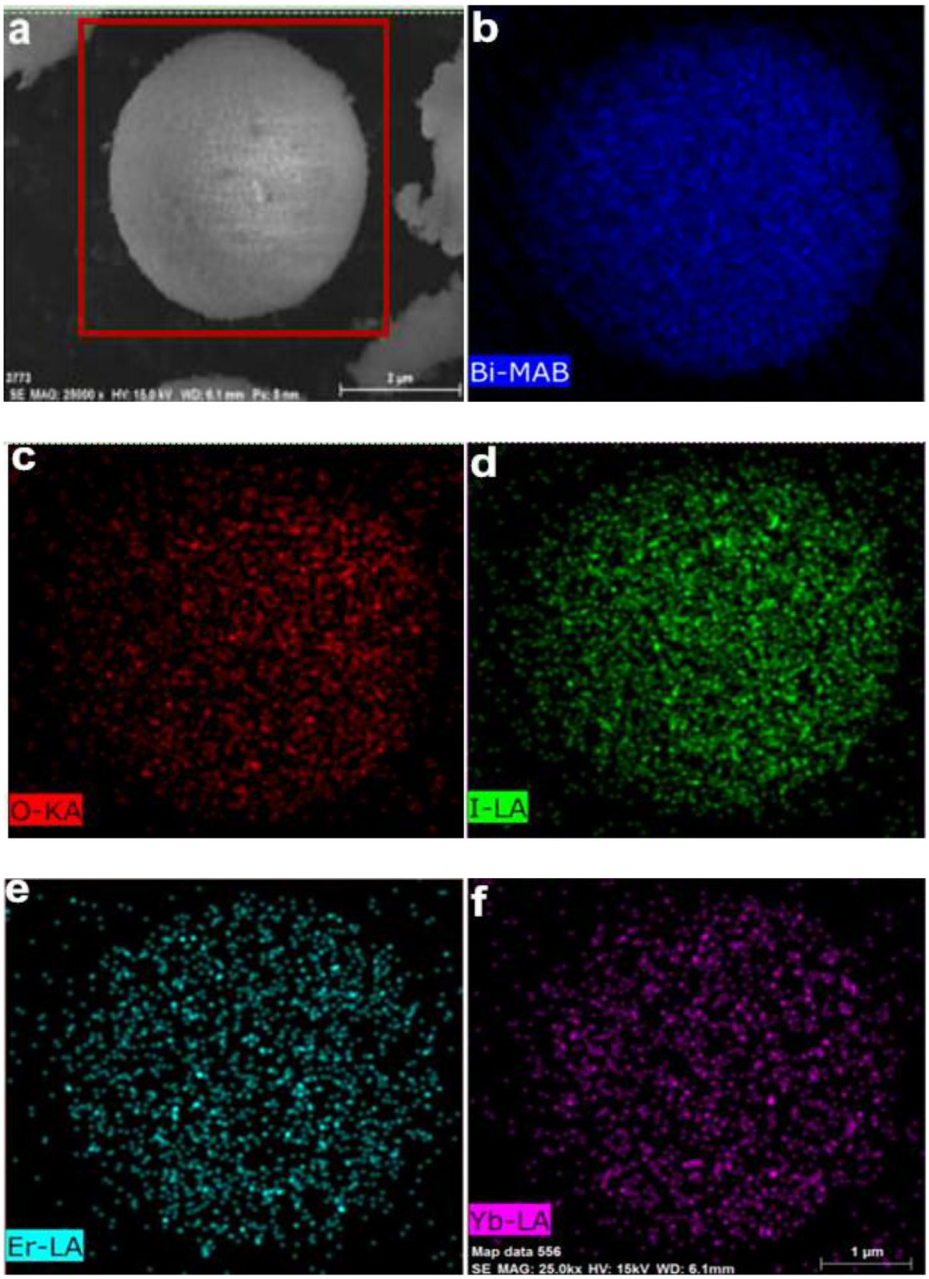

FIGURE 3 | SEM image **(a)**, Bi **(b)**, O **(c)**, I **(d)**, Er **(e)**, and Yb **(f)** EDS mapping images of 6Y6EBOI sample.

SEM image shows these spheres are stacked by numerous nanosheets. While **Figures 2c–f** show the SEM images of 6EBOI and 6Y6EBOI samples, respectively. The Yb^{3+}/Er^{3+} doping has little effect on the morphology, and all the as-prepared samples also have the uniform porous spherical morphology. Energy dispersive spectrometer (EDS) mapping was performed further to analyze the elemental distribution in the 6Y6EBOI sample (**Figure 3**). It is observed that the

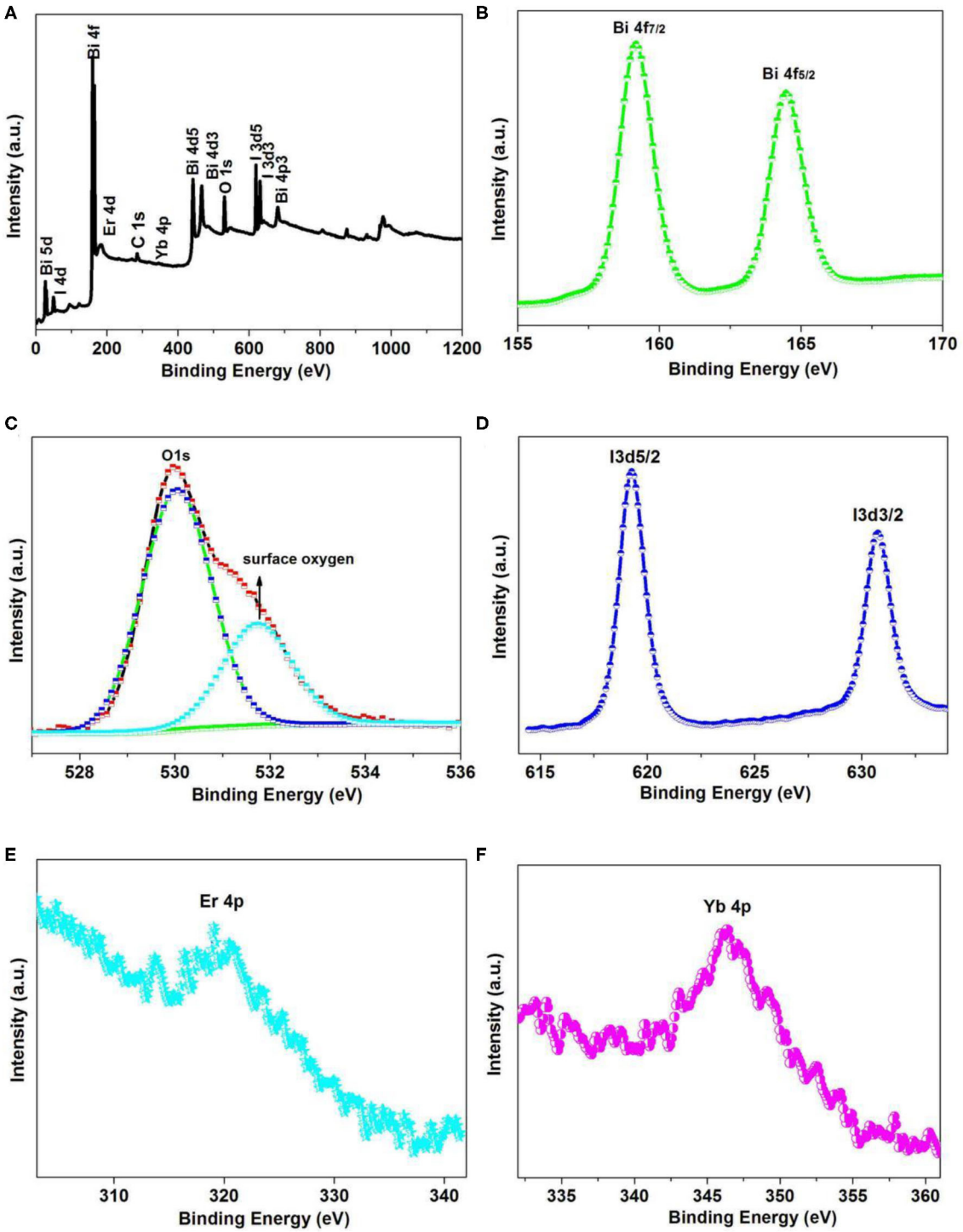

FIGURE 4 | Survey XPS spectra **(A)**, high-resolution XPS spectra of **(B)** Bi 4f, **(C)** O 1s, **(D)** I 3d, **(E)** Er 4p, and **(F)** Yb 4p of the 6Y6EBOI sample.

Bi, O, I, Er, and Yb elements are well distributed over the whole microsphere.

XPS Analysis

In order to investigate the elemental composition, XPS analysis was performed on the 6Y6EBOI sample, and the consequences are presented in **Figure 4**. The survey spectrum in **Figure 4A** clearly reveals the compound consists of Bi, O, I, Er, and Yb elements. There are two peaks at ∼164.4 and 158.9 eV (**Figure 4B**), which are ascribed to Bi $4f_{7/2}$ and Bi $4f_{5/2}$ (Liu et al., 2017), respectively. In **Figure 4C**, it is observed that the O 1s peak is located at 529.5 and 531.4 eV, which corresponds to the lattice oxygen and surface-adsorbed oxygen in the prepared sample (Zhu et al., 2019). The peaks located at 619.4 and 630.6 eV (**Figure 4D**) correspond with the I $3d_{5/2}$ and I $3d_{3/2}$ (Rao et al., 2019). It is also seen that the Er 4p (**Figure 4E**) and Yb 4p (**Figure 4F**) peaks are located at 321.1 and 346.5 eV, which corresponds with the Er^{3+} and Yb^{3+} (Hou et al., 2012; Reszczynska et al., 2015), respectively. Thus, the XPS results indicate that the Er^{3+} and Yb^{3+} were triumphantly doped into the Bi_5O_7I sample.

Ultraviolet-vis DRS Analysis

The ultraviolet–visible (UV-vis) absorption spectra of the prepared samples are depicted in **Figure 5**. The adsorption edge of pure BOI is shorter than 450 nm, indicating that pristine BOI could be excited by the ultraviolet light and a small fraction of visible light. Compared with pure BOI, the visible light absorption of Yb^{3+}/Er^{3+}-doped BOI samples undergoes a significant redshift. It can be seen that three peaks are located

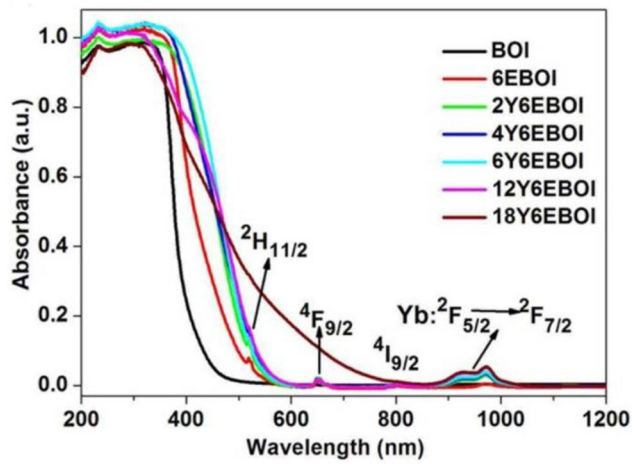

FIGURE 5 | UV-vis adsorption spectra of synthesized pure BOI, 6E BOI, and $Yb^{3+}/6\%Er^{3+}$ co-doped Bi_5O_7I photocatalysts.

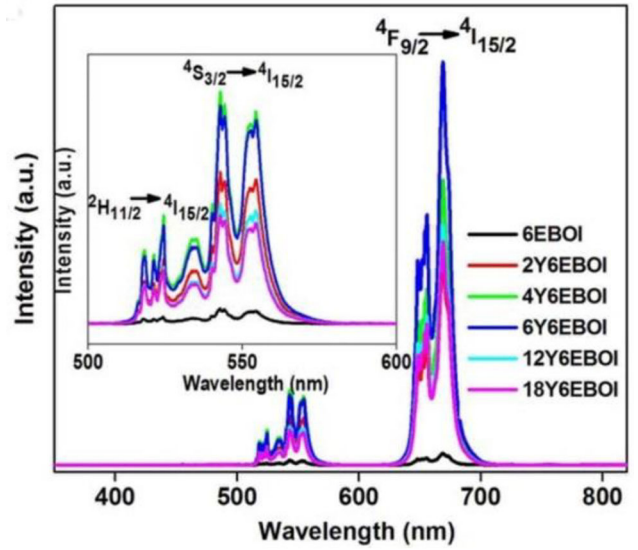

FIGURE 6 | Upconversion spectra of Er^{3+}-doped Bi_5O_7I; and Yb^{3+}-Er^{3+}co-doped Bi_5O_7I sample under 980-nm laser excitation.

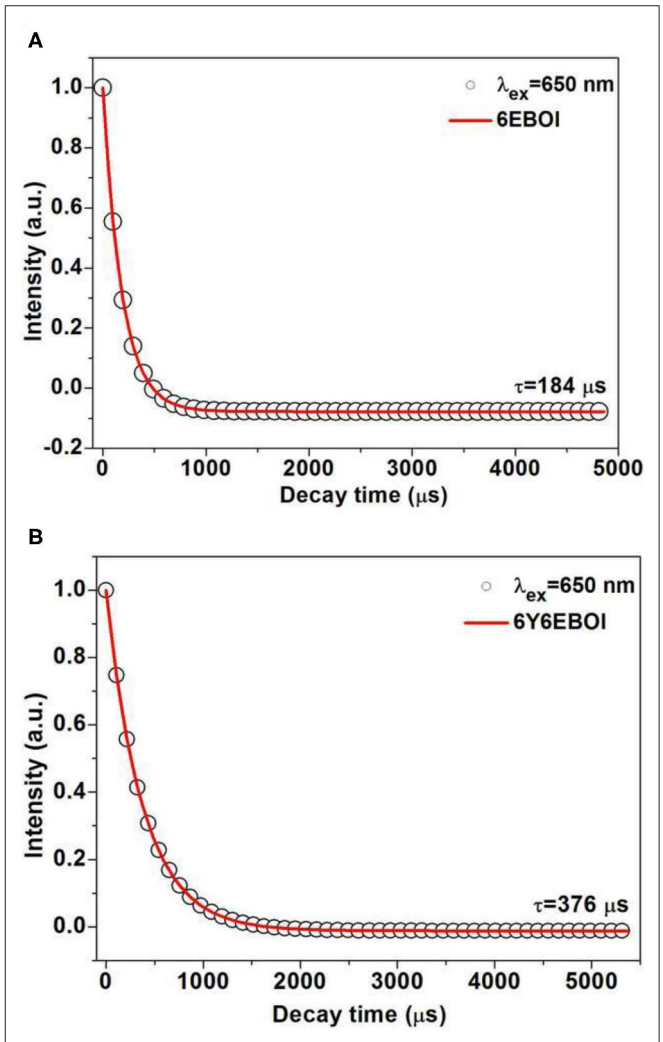

FIGURE 7 | Decay curves of $^4F_{9/2}$-$^4I_{15/2}$ transitions of Er^{3+} ions for the corresponding 6EBOI **(A)** and 6Y6EBOI **(B)** samples.

at 522, 655, and 797 nm for 6EBOI. This is attributed to the upconversion effect from the $^4I_{15/2}$ ground state to $^2H_{2/11}$, $^4F_{9/2}$, and $^4I_{9/2}$ states of Er^{3+} (Rodríguez et al., 2013; Xu et al., 2014). An exception absorption peak at nearly 950 nm for the Yb^{3+}-doped 6EBOI sample is also clearly observed, which is attributed to the upconversion conversion from the $^2F_{5/2}$ ground state to $^2F_{7/2}$ states of Yb^{3+} (Wang et al., 2014).

In order to know the cause of these new peaks in the visible and near IR (NIR) light range, the upconversion spectra of YEBOI samples were carried out. **Figure 6** exhibits the UC emission spectra (350–800 nm) of YEBOI samples. It shows that there are two green emission bands near 533 and 547 nm, and a red emission band near 654 nm after excitation by an NIR laser ($\lambda = 980$ nm). The former between 515 to 538 nm and 540 to 560 nm are ascribed to the $^2H_{11/2} \rightarrow {}^4I_{15/2}$ and $^4S_{3/2} \rightarrow {}^4I_{15/2}$ transitions (Zhang et al., 2005; Sun et al., 2011; Mahalingam et al., 2013). The latter between 640 and 680 nm corresponds with the transition of $^4F_{9/2}$ to $^4I_{15/2}$. It is very clear that the intensity of the green and red emission bands increases over Yb^{3+}-doped 6EBOI sample. Therefore, the observation results indicate that the new absorption bands appearing in the UV-vis DRS spectra are caused by the upconversion radiation of the YEBOI system (Liu et al., 2013; Bai et al., 2014; Zhou et al., 2015). It is well-known that the lifetime of the upconversion materials exhibits a positive correlation with the upconversion quantum yield (Dai et al., 2013). Thus, the luminescence decay curves of the as-synthesized 6EBOI and 6Y6EBOI are also compared under the excitation light with 650 nm wavelength (**Figure 7**). The decay curves of 6EBOI and 6Y6EBOI are 184 and 376 μs, respectively. Hence, the lifetime is significantly prolonged after Yb^{3+}dopping compared with the 6EBOI sample. It is concluded that the tendency of lifetime variation is consistent with that of upconversion intensity variation.

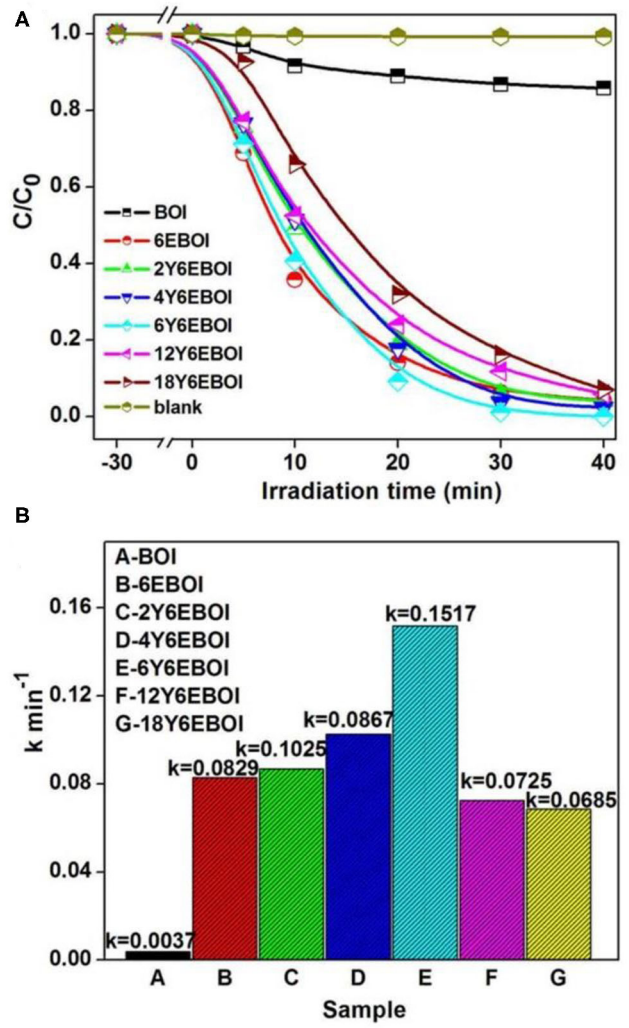

FIGURE 8 | Variation of BPA concentration (C/C_0) against photodegradation time **(A)** and photocatalytic reaction rate constant k **(B)** of BOI, 6EBOI and Yb^{3+}/Er^{3+} co-doped Bi_5O_7I samples.

Photo-Degradation of Bisphenol A

Bisphenol A (BPA) in aqueous solution is selected as target to be degraded, and the photocatalytic efficiency of the photocatalysts under visible light irradiation is shown in **Figure 8**. As indicated in **Figure 8A**, after visible light irradiation for 40 min, the photocatalytic rates of BOI, 6EBOI, 2Y6EBOI, 4Y6EBOI, 6Y6EBOI, 12Y6EBOI, and 18Y6EBOI are 14.1, 95.7, 95.9, 97.7, 100, 94.1, and 92.9, respectively. Therefore, the 6Y6EBOI sample shows the best photocatalytic performance of all the as-prepared samples in this work. According to the Langmuir–Hinshelwood kinetics model (Chen et al., 2012), the below formula is used to express the degradation process:

$$\ln (C_1/C) = \mathrm{kt} \quad (1)$$

where C_1 represents the amount of target removal object after the equilibrium is reached between adsorption and desorption ($t = 0$), and C represents the real-time concentration of the degradation (t). As shown in **Figure S1**, the k's for BOI, 6EBOI, 2Y6EBOI, 4Y6EBOI, 6Y6EBOI, 12Y6EBOI, and 18Y6EBOI samples were calculated as approximately 0.0037, 0.0829, 0.0867, 0.1025, 0.1517, 0.0725, and 0.0685 min^{-1} (**Figure 8B**), respectively. The kinetic results for pristine BOI, 6EBOI, and 6Y6EBOI samples prove the remarkable enhancement photocatalytic efficiency after Yb^{3+} and Er^{3+} doping into BOI photocatalysts.

The photocatalytic activities of BOI, 6EBOI, 2Y6EBOI, 4Y6EBOI, 6Y6EBOI, 12Y6EBOI, and 18Y6EBOI samples under different wavelengths of monochromatic light were also studied. As shown in **Figure 9**, only 4 and 0.3% BPA was degraded under green (G) and red (R) light irradiation for 125 min over BOI, respectively. In particular, the degradation efficiencies of 6EBOI, 2Y6EBOI, 4Y6EBOI, 6Y6EBOI, 12Y6EBOI, and 18Y6EBOI samples are 69.8, 92.1, 93.6, 95.5, 81.1, and 77.3 (**Figure 9A**) under green light irradiation for 125 min, respectively. The degradation efficiencies of 6EBOI, 2Y6EBOI, 4Y6EBOI, 6Y6EBOI, 12Y6EBOI, and 18Y6EBOI samples are 4.8, 5.7, 10.1, 8.1, 6.4, and 5.9% under the red light irradiation for 125 min, respectively (**Figure 9B**). The k's of BOI, 6EBOI,

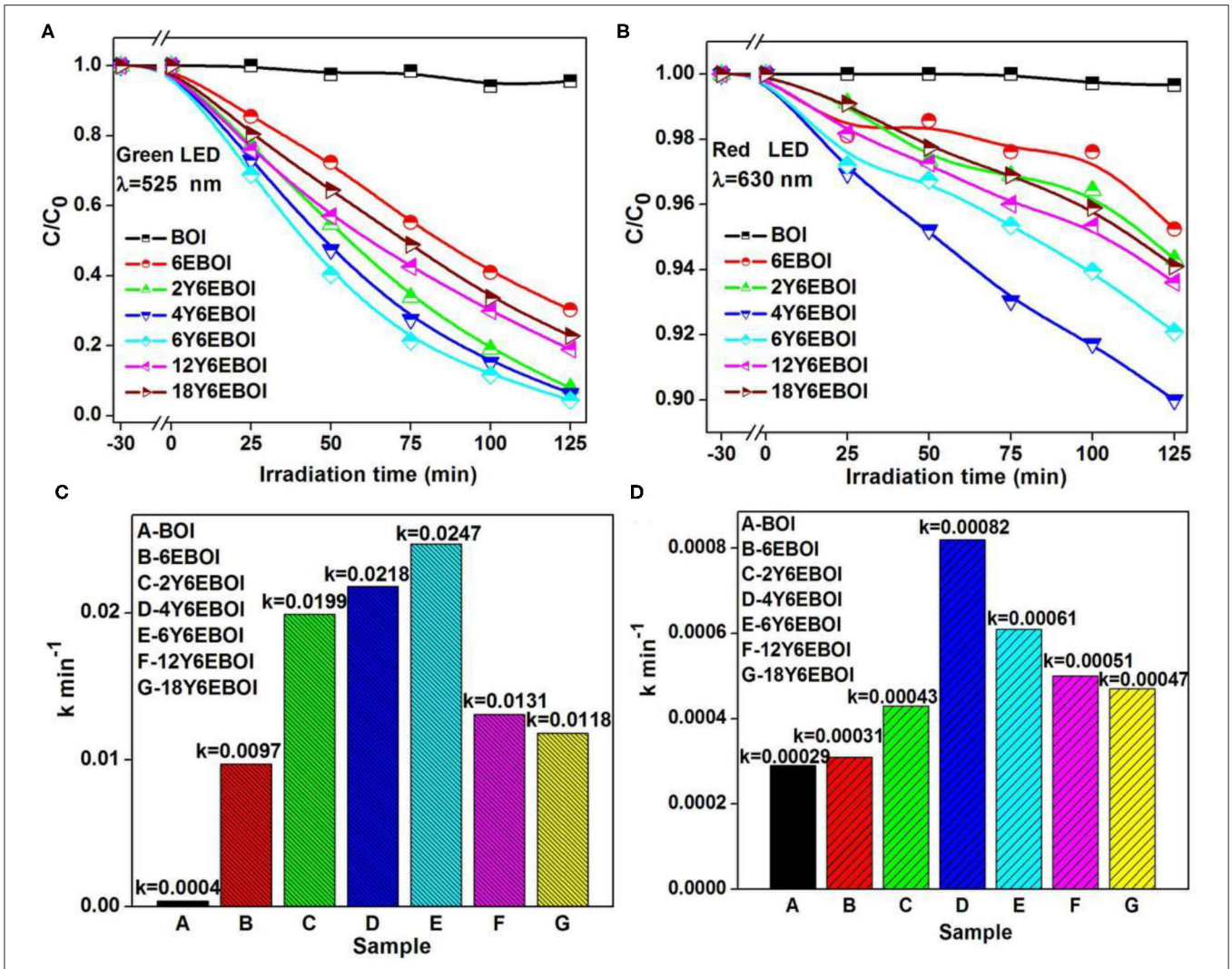

FIGURE 9 | The photocatalytic activities of the Er^{3+}-doped Bi_5O_7I **(A,C)** and Yb^{3+}/Er^{3+}-doped Bi_5O_7I **(B,D)** sample under different wavelength monochromatic light irradiation.

2Y6EBOI, 4Y6EBOI 6Y6EBOI, 12Y6EBOI, and 18Y6EBOI samples calculated from the data were 0.0004, 0.0097, 0.0199, 0.0218, 0.0247, 0.0131, and 0.0188 min^{-1} in **Figure 9C** under green light irradiation, and 0.00029, 0.00031, 0.00043, 0.00082, 0.00061, 0.00050, and 0.00047 min^{-1} in **Figure 9D** under the illumination of red light, respectively. These results indicate that the 6Y6EBOI sample has the most excellent photocatalytic performance for BPA degradation than pure BOI, 6EBOI, and other Er^{3+}/Yb^{3+} co-doped BOI samples.

Apparently, the photocatalytic activity was greatly improved after the doping of Yb^{3+} and Er^{3+} with Bi_5O_7I under visible light irradiation. It is more interesting that the 6Y6EBOI also possesses the best photocatalytic activity under NIR light (940 nm LED light) irradiation. For comparison, BOI and 6EBOI were also used as reference photocatalysts under the same experimental condition. As exhibited in **Figures 10A,B**, the photodegradation efficiencies of BOI, 6EBOI, and 6Y6EBOI samples are 0.3, 1.8, and 9.4%, respectively. The characteristic peak of BPA does not show any change even when the irradiation time reached 60 min over the BOI sample (**Figure 10C**). However, it has an obvious decrease of the peak intensity at 277 nm of BPA with the addition of 6E6YBOI sample as shown in **Figure 10D**. From the above photocatalytic results, the photocatalytic activity of the 6E6YBOI photocatalyst has excellent photocatalytic performance under visible light and NIR light irradiation.

PL Spectra and *I-V* Analysis

The transient photocurrent (*I-V*) and PL are effective tests in displaying the separation ability of photo-generated carriers in photocatalytic research (Chang et al., 2019; Li et al., 2020a). The responses of *I-V* for BOI, 6EBOI, and 6Y6EBOI were also recorded under visible light irradiation. As shown in **Figure 11A**, the intensity of photocurrent signal of 6E6FBOI is much stronger than the pristine BOI and 6EBOI, which

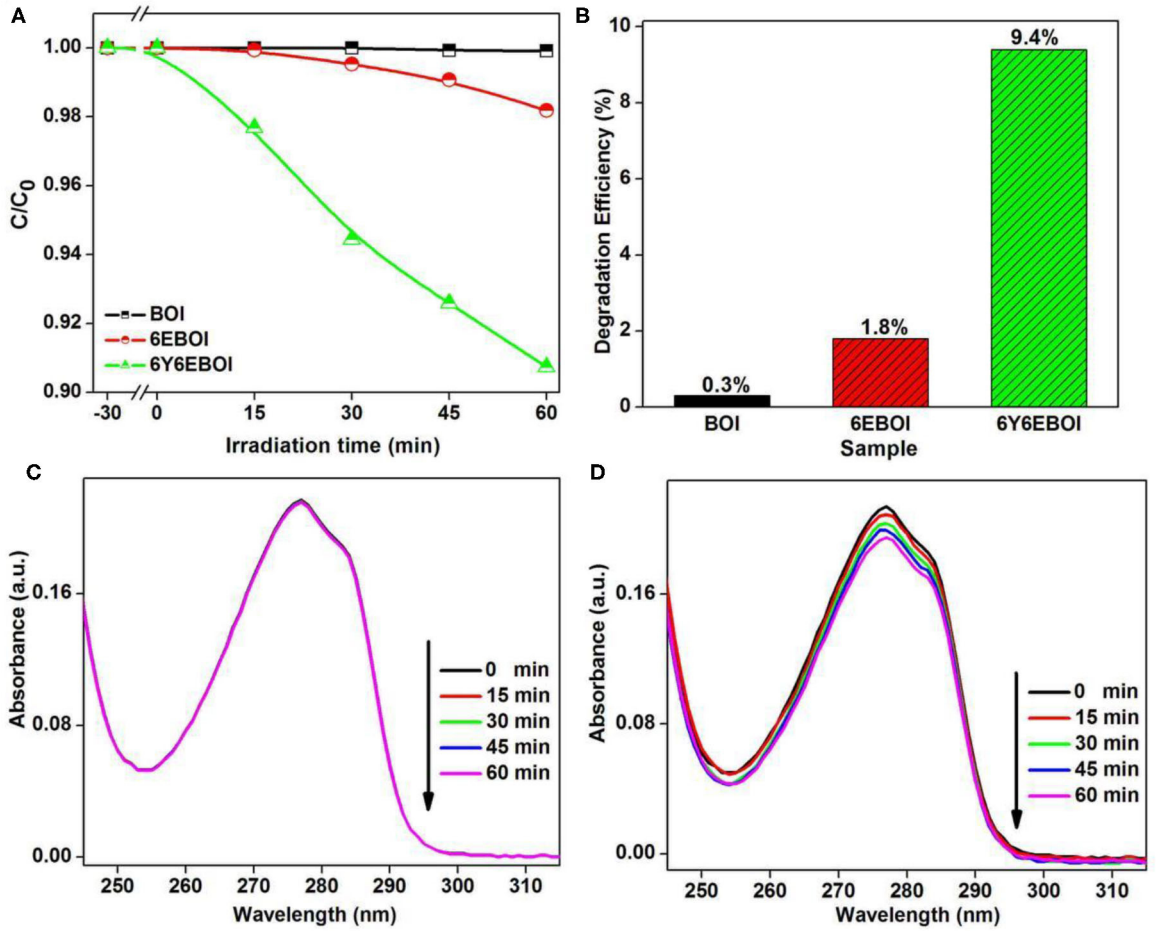

FIGURE 10 | The photocatalytic activities **(A)** and degradation rate **(B)** of the BOI, 6EBOI, and 6Y6EBOI samples under 940-nm LED light irradiation, the variation of UV-vis spectral for the BPA in aqueous solution of BOI **(C)**, and 6Y6EBOI **(D)** samples.

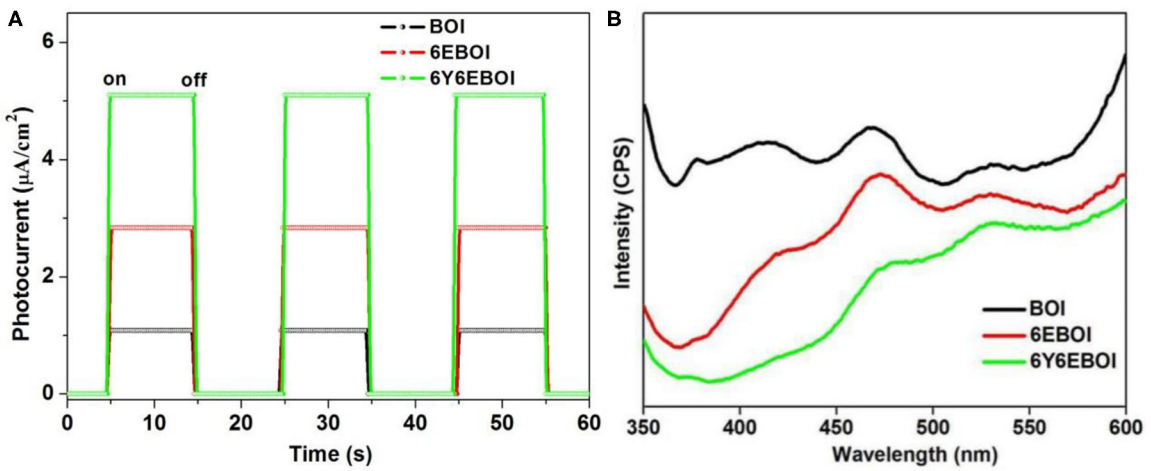

FIGURE 11 | Transient photocurrent **(A)** and PL spectra **(B)** of the BOI, 6EBOI, and 6Y6EBOI samples.

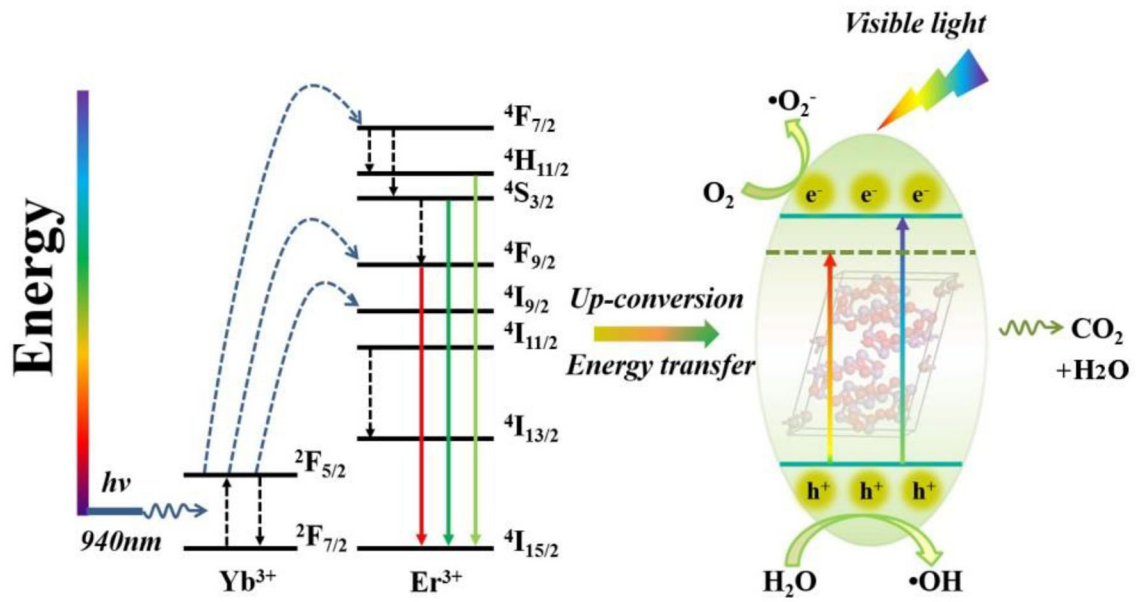

FIGURE 12 | Schematic photodegradation mechanisms over 6Y6EBOI sample under visible light irradiation.

suggests the best excellent effective transfer ability of photo-induced charge carriers. The PL spectra were also carried out to probe the recombination of photo-generated charge carriers (Li et al., 2020b; Nie et al., 2020). Compared with BOI and 6EBOI samples, the lowest intensity of 6Y6EBOI suggests that it possesses the lowest recombination rate of photo-generated charge carriers, which is beneficial to improve the photocatalytic activity (**Figure 11B**). According to above results, the Er^{3+} and Yb^{3+} doping into Bi_5O_7I samples shows enhancing photocatalytic degradation activities for BPA.

Photocatalytic Mechanism

Figure 12 illustrates the photocatalytic reaction mechanism of the Yb^{3+}/Er^{3+}-doped Bi_5O_7I photocatalyst. It can be seen that the Yb^{3+}/Er^{3+}-doped Bi_5O_7I sample could absorb low-energy IR light, and then the electrons would be excited from the level of $^2F_{7/2}$ to $^2F_{5/2}$. Then, the excited electrons would be transferred back to the ground state of $^2F_{7/2}$, and the energy released in this process is mainly transferred to the active Er^{3+} in a non-radiative manner, leading to a population of Er^{3+} from $^4I_{15/2}$ to $^4I_{11/2}$ (Wu et al., 2013). Next, a second or more similar photons from excited Yb^{3+} may convert to higher $^4F_{9/2}$, $^4F_{7/2}$, and $^2I_{9/2}$ energetic levels of Er^{3+}. Then, some of the excited electrons will relax non-radiatively to the energy levels of $^2H_{11/2}$, $^4S_{3/2}$, $^4F_{9/2}$ etc. energy levels through a fast multiphonon decay process (Lei et al., 2015), leading to a stronger green ($^2H_{11/2}$, $^4S_{3/2}$-$^4I_{15/2}$) and red emission ($^4F_{9/2}$-$^4I_{15/2}$), especially the latter. Therefore, the improvement in photocatalytic efficiency of the YEBOI samples could be elaborated more clearly in three factors. First, the Yb^{3+}/Er^{3+}doping in the photocatalyst can cause significant redshift with the absorption of visible light, which would excite more electron-hole pairs. Second, the upconversion process in Yb^{3+}/Er^{3+}-doped Bi_5O_7I sample will take place, and it will produce electron-hole pairs under low-energy IR light irradiation. In this process, the photoactivity of Yb^{3+}/Er^{3+}-doped Bi_5O_7I sample is evidently enhanced. Third, the Yb^{3+} and Er^{3+} in the Bi_5O_7I would promote the separation of e^-/h^+ pairs, so more photo-induced charge carriers would migrate to the sample surface for photocatalytic reaction (Zhang et al., 2012).

CONCLUSIONS

In this work, the Yb^{3+}/Er^{3+}-doped Bi_5O_7I microsphere photocatalysts were prepared through combining hydrothermal and heat-treatment method. The Yb^{3+}/Er^{3+}-doped Bi_5O_7I photocatalysts have excellent photocatalytic for BPA under visible light irradiation and upconversion luminescence properties. It is expected that the synthetic method and properties of this catalyst will offer some inspiration and help for the future researchers to improve similar photocatalytic and upconversion luminescence materials.

DATA AVAILABILITY STATEMENT

The raw data supporting the conclusions of this article will be made available by the authors, without undue reservation.

AUTHOR CONTRIBUTIONS

GZ designed the project. BC, SG, and LL performed the experiments. BC, SG, and RD performed the data analysis. GZ, YX, and LG contributed to the theoretical analysis. BC,

SG, and SZ wrote the paper. All authors contributed to the general discussion, contributed to the article, and approved the submitted version.

FUNDING

This work was supported by the National Natural Science Foundation of China (Grant no. 51772183), the Key Research and Development Program of Shaanxi Province (Grant nos. 2020QFY05-04 and 2018ZDCXL-SF-02-04), and the Fundamental Research Funds for the Central Universities (Grant nos. GK201903023 and GK201801005).

SUPPLEMENTARY MATERIAL

The Supplementary Material for this article can be found online at: https://www.frontiersin.org/articles/10.3389/fchem.2020.00773/full#supplementary-material

REFERENCES

Bai, Z. H., Lin, H., Johnson, J., Gui, S. C. R., Imakita, K. J., Montazami, R., et al. (2014). The single-band red upconversion luminescence from morphology and size controllable Er^{3+}/Yb^{3+} doped MnF_2 nanostructures. *J. Mater. Chem. C* 2, 1736–1741. doi: 10.1039/c3tc32143f

Chang, L. B., Zhu, G. Q., Hassan, Q., Cao, B. W., Li, S. P., Jia, Y. F., et al. (2019). Synergetic effects of Pd^0 metal nanoparticles and Pd^{2+} ions on enhanced photocatalytic of $ZnWO_4$ nanorods for nitric oxide removal. *Langmuir* 35, 11265–11274. doi: 10.1021/acs.langmuir.9b01323

Chen, L., Yin, S. F., Luo, S. L., Huang, R., Zhang, Q., and Hong, T. (2012). $Bi_2O_2CO_3$/BiOI photocatalysts with heterojunctions highly efficient for visible-light treatment of dye-containing wastewater. *Ind. Eng. Chem. Res.* 51, 6760–6768. doi: 10.1021/ie300567y

Chuai, X., Guo, X., Liu, X., He, G., Zheng, K., He, C., et al. (2015). Bifunctional $NaGdF_4$:Yb, Er, Fe nanocrystals with the enhanced upconversion fluorescence. *Opt. Mater.* 44, 13–17. doi: 10.1016/j.optmat.2015.02.019

Dai, Y., Xiao, H., Liu, J., Yuan, Q., Ma, P. A., Yang, D., et al. (2013). In vivo multimodality imaging and cancer Therapy by near-infrared light-triggered trans-Platinum pro-drug-conjugated upconverison nanoparticles. *J. Am. Chem. Soc.* 135, 18920–18929. doi: 10.1021/ja410028q

Ding, M. Y., Chen, D. Q., Ma, D. Y., Dai, J. B., Li, Y. T., and Ji, Z. G. (2016). Highly enhanced upconversion luminescence in lanthanide-doped active-core/luminescent-shell/ active-shell nanoarchitectures. *J. Mater. Chem. C* 4, 2432–2437. doi: 10.1039/C6TC00163G

Fu, J. X., Zhang, X. Z., Chao, Z. C., Li, Z. B., Liao, J. S., Hou, D. J., et al. (2017). Enhanced upconversion luminescence of $NaYF_4$:Yb, Er microprisms via La^{3+} doping. *Opt. Laser. Technol.* 88, 280–286. doi: 10.1016/j.optlastec.2016.09.029

Hojamberdiev, M., Zhu, G. Q., Li, S. P., Zhang, Y. F., Gao, J. Z., Zhu, R. L., et al. (2020). Er^{3+}-doping induced formation of orthorhombic/monoclinic Bi_5O_7I heterostructure with enhancing visible-light photocatalytic activity for removal of contaminants. *Mater. Res. Bull.* 123, 110701–110712. doi: 10.1016/j.materresbull.2019.110701

Hou, D. X., Gei, R., Wang, X. P., Wang, P. H., and Lim, T. T. (2012). Preparation of carbon-sensitized and Fe-Er codoped TiO_2 with response surface methodology for bisphenol A photocatalytic degradation under visible-light irradiation. *Appl. Catal. B Environ.* 126, 121–133. doi: 10.1016/j.apcatb.2012.07.012

Huang, W. J., Lu, C. H., Jiang, C. F., Wang, W., Song, J. B., Ni, Y. R., et al. (2012). Controlled synthesis of $NaYF_4$ nanoparticles and upconversion properties of $NaYF_4$:Yb, Er(Tm)/FC transparent nanocomposite thin films. *J. Colloid Interface Sci.* 376, 34–39. doi: 10.1016/j.jcis.2012.02.047

Lan, M., Zheng, N., Dong, X. L., Hua, C. H., Ma, H. C., and Zhang, X. F. (2020). Bismuth-rich bismuth oxyiodide microspheres with abundant oxygen vacancies as an efficient photocatalyst for nitrogen fixation. *Dalton Trans.* 49, 9123–9129. doi: 10.1039/D0DT01332C

Lei, P. P., Zhang, P., Yuan, Q. H., Wang, Z., Dong, L. L., Song, S. Y., et al. (2015). Yb^{3+}/Er^{3+}-codoped Bi_2O_3 nanospheres: probe for upconversion luminescence imaging and bbinary contrast agent for computed tomography imaging. *ACS Appl. Mater. Interfaces* 7, 26346–26354. doi: 10.1021/acsami.5b09990

Li, S. J., Chen, J. L., Hu, S. W., Jiang, W., Liu, Y. P., and Liu, J. S. (2020b). A novel 3D Z-scheme heterojunction photocatalyst: $Ag_6Si_2O_7$ anchored on flower-like Bi_2WO_6 and its excellent photocatalytic performance for the degradation of toxic pharmaceutical antibiotics. *Inorg. Chem. Front.* 7, 529–541. doi: 10.1039/C9QI01201J

Li, S. J., Chen, J. L., Hu, S. W., Wang, H. L., Jiang, W., and Chen, X. B. (2020a). Facile construction of novel Bi_2WO_6/Ta_3N_5 Z-scheme heterojunction nanofibers for efficient degradation of harmful pharmaceutical pollutants. *Chem. Eng. J.* 402:126165. doi: 10.1016/j.cej.2020.126165

Li, Z., Li, C., Mei, Y., Wang, L., Du, G., and Xiong, Y. (2013). Synthesis of rhombic hierarchical YF_3 nanocrystals and their use as upconversion photocatalysts after TiO_2 coating. *Nanoscale* 5, 3030–3036. doi: 10.1039/c3nr34018j

Lin, M., Zhao, Y., Liu, M., Qiu, M. S., Dong, Y. Q., Duan, Z. F., et al. (2014). Synthesis of upconversion $NaYF_4$:Yb^{3+}, Er^{3+} particles with enhanced luminescent intensity through control of morphology and phase. *J. Mater. Chem. C.* 2, 3671–3676. doi: 10.1039/C4TC00129J

Liu, C. Y., Huang, H. W., Du, X., Zhang, T. R., Tian, N., Guo, Y. X., et al. (2015). *In situ* co-crystallization for fabrication of g-C_3N_4/Bi_5O_7I heterojunction for enhanced visible-light photocatalysis. *J. Phys. Chem. C.* 119, 17156–17165. doi: 10.1021/acs.jpcc.5b03707

Liu, H., Luo, M., Hua, J. C., Zhou, T. F., Chen, R., and Li, J. L. (2013). β-Bi_2O_3 and Er^{3+} doped β-Bi_2O_3 single crystalline nanosheets with exposed reactive {001} facets and enhanced photocatalytic performance. *Appl. Catal. B Environ.* 140–141, 141–150. doi: 10.1016/j.apcatb.2013.04.009

Liu, Y. B., Zhu, G. Q., Gao, J. Z., Hojamberdiev, M., Zhu, R. L., Wei, X. M., et al. (2017). Enhanced photocatalytic activity of $Bi_4Ti_3O_{12}$ nanosheets by Fe^{3+}-doping and the addition of Au nanoparticles: photodegradation of phenol and bisphenol A. *Appl. Catal. B Environ.* 200, 72–82. doi: 10.1016/j.apcatb.2016.06.069

Ma, Y. M., Liu, H. L., Han, Z. Z., Yang, L. B., and Liu, J. H. (2015). Non-ultraviolet photocatalytic kinetics of $NaYF_4$:Yb, Tm@TiO_2/Ag Core@comby shell nanostructures. *J. Mater. Chem. A.* 3, 14642–14650. doi: 10.1039/C5TA03143E

Mahalingam, V., Hazra, C., Naccache, R., Vetrone, F., and Capobianco, J. A. (2013). Enhancing the color purity of the green upconversion emission from Er^{3+}/Yb^{3+} -doped $GdVO_4$ nanocrystals via tuning of the sensitizer concentration. *J. Mater. Chem. C* 1, 6536–6540. doi: 10.1039/c3tc31328j

Nie, J. L., Hassan, Q., Jia, Y. F., Gao, J. Z., Peng, J. H., Lu, J. B., et al. (2020). La-doped $ZnWO_4$ nanorods with enhanced photocatalytic activity for NO removal: effects of La doping and oxygen vacancies. *Inorg. Chem. Front.* 7, 356–368. doi: 10.1039/C9QI01152H

Obregón, S., and Colón, G. (2014a). Heterostructured Er^{3+} doped $BiVO_4$ with exceptional photocatalytic performance by cooperative electronic and luminescence sensitization mechanism. *Appl. Catal. B Environ.* 158–159, 242–249. doi: 10.1016/j.apcatb.2014.04.029

Obregón, S., and Colón, G. (2014b). Improved O_2 evolution from a water splitting reaction over Er^{3+} and Yb^{3+} co-doped tetragonal $BiVO_4$. *Catal. Sci. Technol.* 4, 2042–2050. doi: 10.1039/C4CY00050A

Obregón, S., Lee, S. W., and Colón, G. (2014). Exalted photocatalytic activity of tetragonal $BiVO_4$ by Er^{3+} doping through a luminescence cooperative mechanism. *Dalton Tran.* 43, 311–316. doi: 10.1039/C3DT51923F

Qin, W., Zhang, D., Zhao, D., Wang, L., and Zheng, K. (2010). Near-infrared photocatalysis based on YF_3:Yb^{3+},Tm^{3+}/TiO_2 core/shell nanoparticles. *Chem. Commun.* 46, 2304–2306. doi: 10.1039/b924052g

Rao, F., Zhu, G. Q., Hojamberdiev, M., Zhang, W. B., Li, S. P., Gao, J. Z., et al. (2019). Uniform Zn^{2+}-doped BiOI microspheres assembled by ultrathin nanosheets with tunable oxygen vacancies for super-stable

removal of NO. *J. Phys. Chem. C* 123, 16268–16280. doi: 10.1021/acs.jpcc.9b03961

Reszczynska, J., Grzybb, T., Sobczak, J. W., Lisowski, W., Gazdad, M., Ohtanie, B., et al. (2015). Visible light activity of rare earth metal doped (Er^{3+}, Yb^{3+} or Er^{3+}/Yb^{3+}) titania photocatalysts. *Appl. Catal. B Environ*. 163, 40–49. doi: 10.1016/j.apcatb.2014.07.010

Rodríguez, V. D., Tikhomirov, V. K., Velázquez, J. J., Shestakov, M. V., and Moshchalkov, V. V. (2013). Visible-to-UV/Violet upconversion dynamics in Er^{3+}-doped oxyfluoride nanoscale glass ceramics, *Adv. Opt. Mater*. 1, 747–752. doi: 10.1002/adom.201300212

Sun, J., Xian, J., and Du, H. (2011). Hydrothermal synthesis of $BaYF_5$:Yb^{3+}/Er^{3+} upconversion luminescence submicrospheres by a surfactant-free aqueous solution route. *J. Phys. Chem. Solids* 72, 207–213. doi: 10.1016/j.jpcs.2010.12.013

Wang, W., Huang, W. J., Ni, Y. R., Lu, C. H., Tan, L. J., and Xu, Z. Z. (2013). Graphene supported β-$NaYF_4$:Yb^{3+},Tm^{3+} and N-doped P25 nanocomposite as an advanced NIR and sunlight driven upconversion photocatalyst. *App. Surf. Sci*. 282, 832–837. doi: 10.1016/j.apsusc.2013.06.066

Wang, Y. F., Xu, W., Zhu, Y. S., Xu, S., Cui, H. N., and Song, H. W. (2014). Phonon-modulated upconversion luminescence properties in some Er^{3+} and Yb^{3+} co-activated oxides. *J. Mater. Chem. C* 2, 4642–4650. doi: 10.1039/c4tc00330f

Wu, X. Y., Yin, S., Dong, Q., Liu, B., Wang, Y. H., Sekino, T., et al. (2013). UV, visible and near-infrared lights induced NO_x destruction activity of (Yb,Er)-$NaYF_4$/C-TiO_2 composite. *Sci. Rep*. 3, 2911–2918. doi: 10.1038/srep02918

Xu, D. X., Lian, Z. W., Fu, M. L., Yuan, B. L., Shi, J. W., and Cui, H. J. (2013). Advanced near-infrared-driven photocatalyst: fabrication, characterization, and photocatalytic performance of β-$NaYF_4$:Yb^{3+},Tm^{3+}@TiO_2 core@shell microcrystals. *Appl. Catal. B Environ*. 142–143, 377–386. doi: 10.1016/j.apcatb.2013.05.062

Xu, J. S., Brenner, T. J. K., Chen, Z. P., Neher, D., and Antonietti, M. (2014). Upconversion-agent induced improvement of g-C_3N_4 photocatalyst under visible light. *ACS Appl. Mater. Interfaces* 6, 16481–16486. doi: 10.1021/am5051263

Zhang, J., Dai, S., Wang, G., Zhang, L., Sun, H., and Hu, L. (2005). Investigation on upconversion luminescence in Er^{3+}/Yb^{3+}codoped tellurite glasses and fibers. *Phys. Lett. A* 345, 409–414. doi: 10.1016/j.physleta.2005.07.014

Zhang, J. Y., Zhu, G. Q., Li, S. P., Rao, F., Hassan, Q., Gao, J. Z., et al. (2019). Novel Au/La-Bi_5O_7I microspheres with efficient visible-light photocatalytic activity for NO removal: synergistic effect of Au nanoparticles, La doping and oxygen vacancy. *ACS Appl. Mater. Interfaces* 41, 37822–37832. doi: 10.1021/acsami.9b14300

Zhang, L., Wang, W. Z., Sun, S. M., Zhang, Z. J., Xu, J. H., and Ren, J. (2012). Photocatalytic activity of Er^{3+}, Yb^{3+} doped Bi_5O_7I. *Catal. Commun*. 26, 88–92. doi: 10.1016/j.catcom.2012.04.021

Zhang, L. L., Sha, J. N., Chen, R. R., Liu, Q., Liu, J. Y., Yu, J., et al. (2020a). Surface plasma Ag-decorated Bi_5O_7I microspheres uniformly distributed on a zwitterionic fluorinated polymer with superfunctional antifouling property. *Appl. Catal. B Environ*. 271:118920. doi: 10.1016/j.apcatb.2020.118920

Zhang, L. L., Sha, J. N., Chen, R. R., Liu, Q., Liu, J. Y., Yu, J., et al. (2020b). Three-dimensional flower-like shaped Bi_5O_7I particles incorporation zwitterionic fluorinated polymers with synergistic hydration-photocatalytic for enhanced marine antifouling performance. *J. Hazard. Mater*. 389:121854. doi: 10.1016/j.jhazmat.2019.121854

Zhou, J. J., Chen, G. X., Zhu, Y. B., Huo, L. L., Mao, W., Zou, D. N., et al. (2015). Intense multiphoton upconversion of Yb^{3+}-Tm^{3+} doped β-$NaYF_4$ individual nanocrystals by saturation excitation. *J. Mater. Chem. C* 3, 364–369. doi: 10.1039/C4TC02363C

Zhu, G. Q., Li, S. P., Gao, J. Z., Zhang, F. C., Liu, C. L., Wang, Q. Z., et al. (2019). Constructing a 2D/2D $Bi_2O_2CO_3$/$Bi_4O_5Br_2$ heterostructure as a direct Z-scheme photocatalyst with enhanced photocatalytic activity for NO_x removal. *Appl. Surf. Sci*. 493, 913–925. doi: 10.1016/j.apsusc.2019.07.119

Conflict of Interest: The authors declare that the research was conducted in the absence of any commercial or financial relationships that could be construed as a potential conflict of interest.